Industrial Crops & Products 201 (2023) 116895

Contents lists available at ScienceDirect

Industrial Crops & Products

journal homepage: www.elsevier.com/locate/indcrop

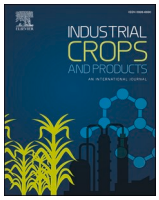

Coir/glass hybrid fiber reinforced thermoset polymer composite laminates with room-temperature self-healing and shape memory functions

Sakil Mahmud [a], John Konlan [a], Jenny Deicaza [b], Guoqiang Li [a,b,*]

[a] Department of Mechanical and Industrial Engineering, Louisiana State University, Baton Rouge, LA 70803, United States
[b] Department of Mechanical Engineering, Southern University and A&M College, Baton Rouge, LA 70813, United States

ARTICLE INFO

Keywords:
Renewable reinforcements
Synthetic fibers
Self-healing
Shape-memory
Composite laminates

ABSTRACT

Natural fibers have a lot of potentials as renewable reinforcements for polymers. However, their lower load-carrying capacity compared with synthetic fibers made it a challenge to use them as polymer reinforcements. When a laminated composite beam is bent, the normal stress is the highest on the top and bottom layers and zero in the midplane due to the (non)linear distribution of normal strain. Even though the shear stress is the highest in the midplane, most polymers can tolerate the high shear stress. Therefore, hybrid composite laminates with strong synthetic glass fibers stacked over the core of weak natural coir fiber reinforcement have been designed. Even using a significant portion of coir fibers in the composites, the samples with hybrid fiber reinforcement showed almost similar mechanical properties compared with the samples with glass fiber reinforcement alone. Delamination and matrix crack induced by low velocity impact inside the composite panels were repeatedly healed at room temperature due to the self-healing capability of the diglycidyl 1,2-cyclohexanedicarboxylate (DCN) and polyethylenimine (PEI) polymer matrix. The healing efficiency was up to 99% for the first healing cycle and 72% for the fourth healing cycle. The composites also had good shape memory properties, with a shape fixity ratio up to 51% and a shape recovery ratio up to 93%, which were well maintained even after the several damage/healing cycles of the composites. This study opens new opportunities for applications of natural fibers in multifunctional load-bearing composites.

1. Introduction

Due to the excellent specific mechanical properties of fiber-reinforced polymer (FRP) composites, they are now an attractive class of structural materials (Mazumdar et al., 2017). They are being utilized frequently as lightweight materials in several industrial fields such as building, automotive, aeronautical, and energy industries (Abrão et al., 2007). Although polymer itself has become a major concern of plastic pollution (MacLeod et al., 2021), these excellent properties have resulted in mass production of polymer composites, which in recent years has led to significant demand for inorganic reinforcement (Shiino et al., 2021). In addition to the graphene oxide (Zhu et al., 2022) and metal microcapsules (Sun et al., 2021), the reinforcement specially made of carbon fibers has particular properties that appeal to the needs of different industries (Forintos and Czigany, 2019). Recently, carbon-based fiber and its composites have been broadly studied as piezoelectric sensors, high-performance microwave absorption materials, lightweight structural materials, treatment of antibiotics, and so on (Sharafkhani and Kokabi, 2022; Zhang et al., 2022). Moreover, like diverse applications of pure polymer ranging from energy materials to water treatment (Ouyang et al., 2022), glass fiber reinforced polymer composite laminates have been extensively used in many other sectors, including the manufacturing of wind turbine blades and nacelles for renewable energy devices (Sathishkumar et al., 2014; Yang et al., 2016). However, waste created during the manufacturing process and end-of-life products, which have several restrictions for landfill disposal, are simultaneously implicated in the expansion and production of composites (Verma et al., 2016). Additionally, the majority of the waste material is made of polymers and inorganic fillers, which could contaminate soil and fresh water, among other negative environmental effects (Li et al., 2021). In order to achieve sustainable development and relieve deep ecological concerns, it has become crucial for all sectors to phase out non-sustainable products in favor of their sustainable counterparts (Monteiro et al., 2009). Therefore, natural fibers come in the frontline as reinforcement in FRP composites instead of synthetic ones. This is due to many advantages of natural fibers over synthetic fibers,

* Corresponding author at: Department of Mechanical and Industrial Engineering, Louisiana State University, Baton Rouge, LA 70803, United States.
E-mail address: lguoqi1@lsu.edu (G. Li).

https://doi.org/10.1016/j.indcrop.2023.116895
Received 12 January 2023; Received in revised form 2 April 2023; Accepted 15 May 2023

including greater impact resistance, higher ductility, lower cost, lower specific gravity, less abrasiveness to equipment, less health hazards, more processing-friendly, less greenhouse gas emissions, recyclable, and CO_2 neutral (Kerni et al., 2020).

Coir is such a natural cellulosic fiber that extracted from the husk of the coconut (Fouladi et al., 2011). Unfortunately, these natural fibers cannot compete with synthetic fibers where mechanical properties are highly desirable (Feni et al., 2022). To solve this problem, hybrid reinforcement in laminated composite beams has been proposed here.

Generally, the normal stress in laminated composite beams is zero under bending load at the midplane, increasing (non)linearly up to the top and bottom layers. Of course, the out-of-plane shear stress is the maximum at the midplane. Fortunately, most polymeric materials can resist this type of shear stress; therefore, this may not be a major concern if the lower-strength materials are used in the vicinity of the midplane. Using this idea as inspiration, we developed a hybrid-style fiber reinforcement in which the strongest fibers are used as top and bottom layers and lower strength natural coir fibers in the midplane.

Many thermoplastic polymers can serve as self-healing materials because once they are melted, they can be remolded and reformed, and thus can heal any cracks or damages that may occur in the material. As a result, thermoplastic particles or fibers have been widely used as healing agent in healing thermoset polymers (Nji and Li, 2010; Nji and Li, 2012). In addition to using thermoplastic as healing agent, a reactive monomer can be incorporated into the polymer matrix, which can polymerize upon damage and restore the material to its original state (Putnam-Neeb et al., 2022). In addition, a reversible phase transition between a crystalline and an amorphous state allows thermoplastic polymers to display shape-memory ability. An external stimulus (e.g., heat, light, etc.) can cause the material to undergo this transition, which causes it to soften and become flexible (Basak, 2021). In contrast, using a crosslinking agent to build a stable network of covalent connections inside the polymer matrix allows thermoset polymers to display shape-memory ability. Subjected to external loading, the network can be deformed into a temporary shape, and when it is exposed to heat or other environmental stimuli, the programmed temporary shape can return to its original shape. Unlike thermoplastic shape-memory polymers, which can use melting temperature as the shape recovery temperature, thermoset shape-memory polymers depend on glass transition temperature to trigger the shape recovery process. Recently, a class of thermoset polymers with self-healing and shape-memory properties has been explored as a matrix for FRP composites (Konlan et al., 2020; Konlan et al., 2022). For example, Chen et al. (2021) studied thermally conductive and intrinsically self-healing glass fiber-reinforced epoxy composites for integrated circuit packaging applications. Such polymers incorporate various dynamic covalent linkages into the crosslinked network that can rearrange by initiating reversible chemical interactions, giving the polymer an inherent capacity for self-healing and recycling (Feng et al., 2019; Feng and Li, 2021a; Li et al., 2018; Lu et al., 2017; Scheutz et al., 2019; Van Zee and Nicolaÿ, 2020). However, in all such polymers, the inflexible crack pathways must first be softened with thermal stimulus or solvent intervention before the self-healing process can begin. In order to apply the self-healing function in most real-world applications, room-temperature self-healing is much more beneficial than healing at elevated temperatures.

Previously diglycidyl 1,2-cyclohexanedicarboxylate (DCN), and polyethylenimine (PEI) based thermoset polymers have been designed to have intrinsic self-healing at room temperature (Feng and Li, 2021b). Of course, other groups have also reported some inherent room-temperature self-healing polymers (Wang et al., 2020b; Xu et al., 2021; Yanagisawa et al., 2018). To defeat the existing obstacle between high-level stiffness and self-healing, they used crosslinking low-molecular-weight (M_w) chains (e.g., linear poly(ether-thiourea), polyurethane, etc.) noncovalently with the weak but intense H-bonds. Consequently, the resultant polymers were repaired at room temperature while being stiff. However, these polymers are still considered as thermoplastics and, therefore, sensitive to heat and chemical solvents (Wang et al., 2020b; Xu et al., 2021; Yanagisawa et al., 2018). In contrast, as-synthesized DCN-PEI network has excessive primary amine ends and secondary amines on the branched chains, which can produce highly intense but loosely packed numerous H-bonds that result in a comparable noncovalent crosslinking network (Feng and Li, 2021b). The produced hydroxyls and the network's intrinsic ester ends can also form reversible covalent bonds at higher temperatures, i.e., self-healable at higher temperatures. These dual crosslinking processes generate a polymer that is both strong mechanically and stable thermally and chemically. Even at room temperature, the excessive flexibility of the chain branches and ends can expedite the reconstruction of the broken H-bonds, leading to room-temperature self-healing of the resulting glassy thermoset. Therefore, the DCN-PEI vitrimer was used as matrix in this study. Another reason for choosing this polymer was due to its dissolving ability in alcohols by catalyst-free transesterification due to the intrinsic catalytic function of the tertiary amines within the system. On the other hand, almost all thermosets with irreversible crosslink structures are unable to be recycled by solvent (Li et al., 2018; Lu et al., 2017; Post et al., 2020), which hinders the possibility of recycling the fibers from laminate composites.

In this present study the influence of the hybrid arrangement of fibers in the laminates, and the number of fibers layers of the woven glass fabrics and coir mats on the restoration of mechanical/functional properties in the composite beams were systematically analyzed. The capability of retaining the inherent properties like shape memory and self-healing behavior in the composites laminate was also investigated.

2. Experimental

2.1. Materials

The branched polyethylenimine (PEI, average $M_w \sim 800$ by LS, average $M_n \sim 600$ by GPC) and epoxy monomer diglycidyl 1,2-cyclohexanedicarboxylate (DCN) were supplied by Sigma-Aldrich (St. Louis, MO, USA). Bidirectional will weave glass fabric was purchased from Fibreglast Developments Corp. USA. The natural coir fibers in a random arrangement in the mat were obtained from Xintai Coir Mat Factory, Xintai, China.

2.2. Preparation of composite laminates

As explained in the previous report (Feng and Li, 2021b), the synthetic route was adopted to prepare the DCN–PEI thermoset. In brief, the branched PEI was mixed with monomer DCN at room temperature, maintaining a mass ratio of 1:1, in a 250-mL beaker. After that, any bubbles produced in the homogenous mixture were entirely removed by degassing them in a vacuum oven for 15 min. The degassed homogenous mixture was then used to wet the cut-out fabrics(165 mm × 165 mm) by hand layup. The wet fibers were then placed in the rectangular open mold of 5.04 mm thickness. Two Teflon sheets and two aluminum plates with an equal dimension as the open mold casing (215 mm × 215 mm) were used to cover the mold and clamped by eight C-clamps. Then the arrangement was kept at room temperature overnight and sent to an oven for two-step thermal curing (100 °C for 2 h and 150 °C for another 2 h). After curing and demolding, the cured panel was cut into 152.40 mm × 25.40 mm × 5.04 mm beams using an electric saw. The entire process is schematically presented in Scheme S1. In addition, the samples were individually prepared with pure coir fibers and glass fabrics as references. They were named natural coir fiber-reinforced polymer (nFRP) composites and glass fiber-reinforced polymer (gFRP) composites, respectively. To prepare the hybrid composites, fibers were arranged in a gradient manner where the midplane was coir fibers, and outer layers were glass fabrics of single, double, and triple layers (marked them nFRP-G1, nFRP-G2, and nFRP-G3, respectively).

2.3. Characterizations and measurements

The composite density (ρ_c) was determined based on Eq. 1 (Mortazavian and Fatemi, 2015), applying the constituent densities from Table 1 and their weight fractions. Scheme 1.

$$\rho_c = \frac{1}{\sum \frac{W_i}{\rho_i}} \tag{1}$$

where ρ_i = density of constituting materials, W_i = weight fraction of constituting materials. Likewise, Eq. 2 was used to determine the volume fractions (V_i) of the fiber and matrix.

$$V_i = W_i \frac{\rho_c}{\rho_i} \tag{2}$$

An MTS Alliance RF/10 machine with 2.0 mm/min loading rate was used to conduct the 3-point bending tests. Eq. 3 and Eq. 4 were used to determine the flexural stress at any point on the load-deflection that occurs at the outer surfaces at the mid-span.

$$\sigma_f = \frac{3PL}{2bh^2} \tag{3}$$

$$\sigma_{s-f} = \frac{\sigma_f}{\rho_c} \tag{4}$$

where σ_f and $\sigma_{s\text{-}f}$ are respectively the flexural stress and specific flexural stress at the outer surface at mid-span, P = applied force, L = span length, b = beam width, and h = beam thickness. Based on the mid-span deflection (δ), Eq. 5 was used to calculate the maximum strain (ε) at the outer surface.

$$\varepsilon = \frac{6\delta h}{L^2} \tag{5}$$

As per standard (ASTM D3763–18), low-velocity impact was conducted on composite using an Instron Dynatup 8250 HV impactor. The impact tests were run in room-temperature, and at least four useful samples were examined for each impact to calculate the mean value and standard deviation. The load and energy traces were used to calculate the maximum impact force, maximum deflection, and impact time. Based on the traces, the initiation and propagation energy were computed.

Using the same 3-point bending instrument the composite sample was bent to 16 mm at a loading rate of 2.0 mm/min at room temperature and held for 10 min to fix the shape. Then the shape fixity ratio (F) and the shape recovery ratio (R) were determined based on calculated length (ℓ) using Eq. 6 and Eq. 7, respectively.

$$F = \frac{\ell_0 - \ell_2}{\ell_0 - \ell_1} \times 100\% \tag{6}$$

Table 1
The formulation of fiber-reinforced polymer composites.

Sample Name	Composite density (g/cm^3)	Glass fiber vol. fraction (%)	Coir fiber vol. fraction (%)	Total Fiber vol. fraction (%)	Matrix vol. fraction (%)
nFRP	1.21	0	25.34	25.34	74.66
gFRP	1.48	23.03	0	23.03	76.97
nFRP-G1	1.27	5.06	19.65	24.71	75.29
nFRP-G2	1.34	11.29	13.20	24.49	75.51
nFRP-G3	1.37	14.09	10.98	25.08	74.92

The density of glass fiber, coir fiber, and DCN-PEI polymer were 2.25 g/cm^3, 1.10 g/cm^3, 1.25 g/cm^3, respectively.

$$R = \frac{\ell_3 - \ell_2}{\ell_0 - \ell_2} \times 100\% \tag{7}$$

where, ℓ_0 = the initial beam length, ℓ_1 = the length after bending, ℓ_2 = the length after the load removal, and ℓ_3 = the length after shape recovery. The repeated 3-point bending tests up to four cycles on healed samples, the repeatability of healing and the healing efficiency based on flexural stress (η_{FS}) was determined using Eq. 8.

$$\eta_{FS} = \frac{\sigma_h}{\sigma_y} \times 100\% \tag{8}$$

where, σ_y = the maximum flexural stress of the virgin specimens, and σ_h = the maximum flexural stress of the healed samples. Similarly, the healing efficiency based on impact force (η_{IF}), and propagation energy (η_{PE}) was determined as follows:

$$\eta_{IF} = \frac{F_{IR}}{F_{I0}} \times 100\% \tag{9}$$

$$\eta_{PE} = \frac{E_P}{E_{P0}} \times 100\% \tag{10}$$

herein, F_{IR} and E_P are the peak impact force and propagation energy of the recycled composite laminate, respectively. F_{I0} and E_{P0} are the maximum impact force and propagation energy of the virgin composite laminate before recycling, respectively.

Attenuated total reflectance Fourier transform infrared spectroscopy (FTIR) of Nicolet 6700 FTIR spectrometer (Thermo Scientific, USA) was used to record the spectra of the composites. The samples were scanned by collecting 32 scans at a resolution of 4 cm^{-1} with a wave number range of 500–4000 cm^{-1}. The delamination and healing in the composites at the macro-length scale were also observed using an Amscope optical microscope.

The thermal properties of the composites were explored using a differential scanning calorimeter (DSC) of Perkin Elmer 4000 (MA, USA) based on the heat-cool-heat technique. About 5 – 10 mg of samples were initially kept at – 50 °C for 2 min and then heated to 200 °C at a rate of 10 °C per/min. They were then kept at 200 °C for 2 min, and cooled to – 50 °C at a rate of – 10 °C/min. After 2 min at – 50 °C, a second scan was conducted at the same heating rate from – 50–200 °C. Throughout the procedure, the sample cell was kept under a nitrogen flow of 30 mL/min. From the second scan, the glass-transition temperature (T_g) was calculated.

To perform non-isothermal thermogravimetric analysis (TGA) tests, TGA550 thermal analyzer (TA instruments, DE, USA) was used. A small amount of sample (~8 mg) was heated from 30 °C to 800 °C at a heating rate of 10 °C /min in a nitrogen (N_2) environment, and the purging rate of the nitrogen gas was 40 mL/min. The temperatures at which 5% of the weight is lost and the peak of the derivative thermogravimetric analysis (DTG) curve were calculated as $T_{d,5\%}$ and $T_{d,max}$, respectively.

3. Results and discussions

3.1. Structural characterizations

Fiber volume fractions (V_f) contribute to the composite's mechanical properties because fibers are the main load-bearing component in a composite. Generally, fiber V_f varies from 10% to 50% in the laminates (Arockiasamy and M, 2022); however, larger fiber volume fractions lead to poor wettability of the fibers by the matrix (Grund et al., 2019). In this study, all composite samples were prepared by maintaining a V_f of ~25% based on typical volume fractions measurement, as given in Table 1.

The FTIR spectra of the pure coir fiber and pure glass fiber are shown in Fig. S1. It is seen that the basic structure of cellulose with a broad peak in the range of 3600–3100 cm^{-1} due to the presence of hydroxyl group

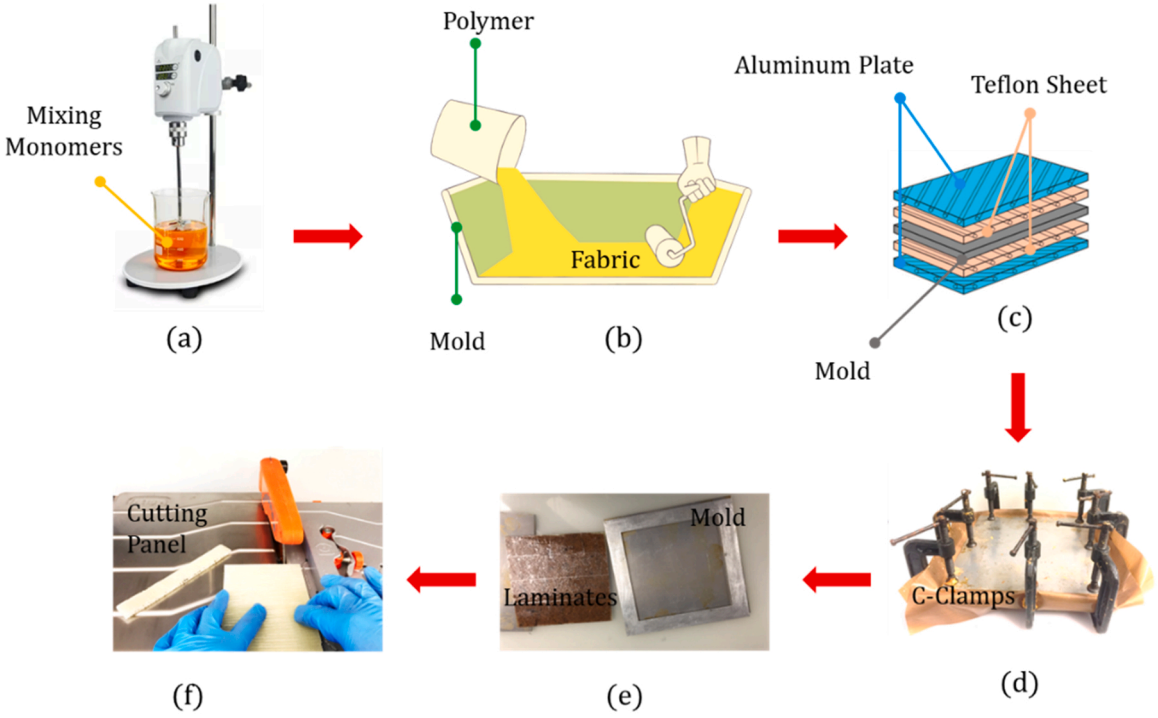

Scheme 1. (a) Mixing of monomers, (b) lamination of fabrics, (c) laminate sandwiched in the mold with aluminum plates covering, (d) C-clamping to exert pressure on laminate, (e) demolding the sandwiched laminate after thermal curing, and (f) cutting of panels into rectangular beams.

and bound O-H stretching vibration in the cellulose and hemicellulose components (Fig. S1). Other major peaks were associated to $–CH_2$ stretching vibration at 2950 cm^{-1}, C═O (carbonyl) in hemicellulose at 1733 cm^{-1}, C-O stretching acetyl group in lignin at 1240 cm^{-1}, and C-O-C stretching of carbohydrate elements of cellulose at 1115 cm^{-1} (Prasad et al., 2018). The FTIR spectra of the pure glass fibers were associated with different types of oxides such as boron oxide, aluminum oxide, etc., the oxygen-silicon bond in the Si–O–Si group at 990 cm^{-1}, and asymmetric deformation vibration of $–CF_3$ group at 682 cm^{-1} (Bonon et al., 2016; Thangaraj et al., 2017). On the other hand, the numerous H-bonds attributable to the –NH, –OH, and C═O groups in the DCN-PEI network are readily seen in the pure polymer (Feng and Li, 2021b).

The FTIR spectra for the pure polymer and the composites are shown in Fig. 1**a**. The remarkable mechanical stiffness of the DCN-PEI thermoset results from the strong H-bonding interfaces and rigid hexatomic rings of DCN. More importantly, the absence of the epoxy group at 902 cm^{-1} indicates complete thermal crosslinking, suggesting the complete curing of the epoxy group. However, the chemical properties of the composites remained unchanged once fiber reinforcements were added (Fig. 1**a**). No new peak appeared, nor existing peak disappeared; even there was no spectral shift was observed in the fiber-reinforced composites. This finding implies that the inclusion of fiber did not change the polymer's chemical composition. This also indicates that there was no chemical bonding between the polymer and the fibers. This common phenomenon is often observed in both natural and synthetic fiber reinforcements if they are not chemically modified or grafted before integration in the polymer matrix (Haafiz et al., 2013; Haris et al., 2021; Rajadurai, 2017). In addition, there were no apparent differences in the FTIR spectra between the pure and hybrid composites. The pure polymer matrix had all the distinguishing bands in the hybrid composites. Based on this, it can be concluded that the chemical characteristics of the composites were unaffected by the hybridization of coir and glass fibers in the matrix. Some researchers have suggested chemically treating the fiber to enhance the chemical bonding and the linkage of the fiber to the matrix. For example, Seghini et al. (2019) specifically performed plasma treatment on reinforcing fiber and discovered some chemical interaction between fibers and polymers.

A second heating DSC scan was used to examine glass transition temperature (T_g), as shown in Fig. 1**b**. The T_g of the pure DCN-PEI thermoset was 36.19 °C, which was increased to 38.38 °C upon the reinforcement of natural coir fibers (nFRP). The increase in T_g was due to the addition of fibers which restricts the movement of polymer chains. The movement restriction is ascribed by some physical interactions or secondary chemical interactions such as hydrogen bonds between the coir fibers and the polymer. In summary, this entitles that interfacial interactions between fibers and polymer permit effective stress transfer from the polymer matrix to the coir fibers. The observations are well matched by theory and mechanism described by Khan et al. (2021). On the other hand, a slight drop in T_g was noticed for gFRP and hybrids composites. This decrease in T_g to the lower temperature may be attributable to the enhanced local mobility of polymer molecules between glass fibers and the matrix (Cho et al., 2009). Another possibility is that the thermal conductivity of the glass fibers is larger than that of the polymer matrix. Therefore, the glass transition begins at lower temperatures.

To determine the thermal degradation of the composite materials, thermogravimetric analysis (TGA) was utilized (Fig. 1**c**). The weight loss and the first derivative of the mass ratio (DTG) with respect to temperature are plotted in Fig. 1**d**. Important factors such as the temperature of 5% weight loss ($T_{5\%}$, the temperature at which degradation began), and the temperature of maximum degradation (T_{max}) are summarized in Table 2. The table shows that the pure polymer and composites were thermally stable up to 180 °C and a maximum ~ 4.0% weight loss was observed at 150 °C; it means the maximum curing temperature (150 °C) used in the synthesis and compositions had no major effect on materials degradation. Based on $T_{5\%}$ and T_{max}, it was observed that other samples exhibited degradation at higher temperatures compared with the pure polymer, demonstrating an increase in thermal stability caused by good fiber-to-matrix adhesion (Reddy et al., 2020). Overall, all samples showed three-step degradation pattern. (1) The sample lost around 1.5% of its original weight from a starting temperature of 25 °C to a temperature of 120 °C, which may be due to

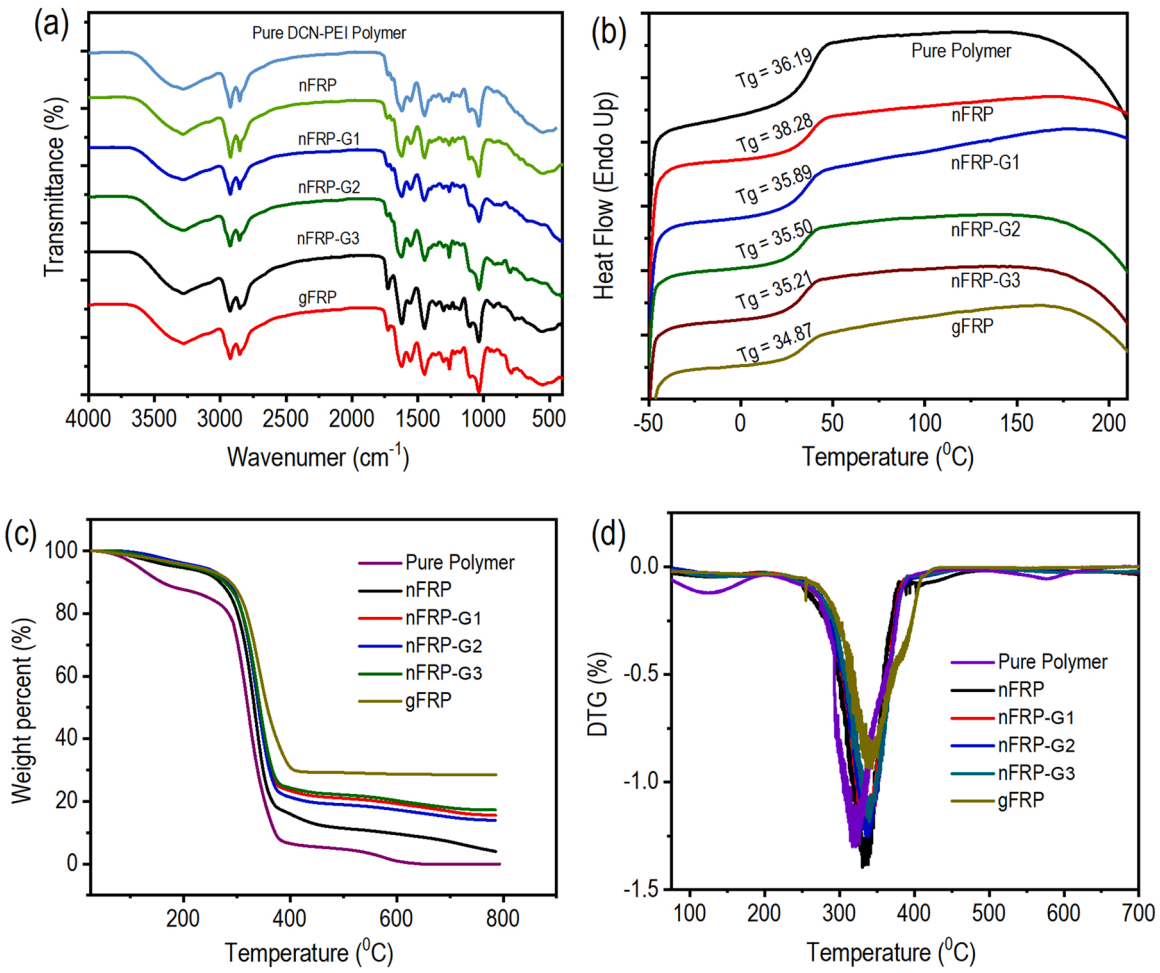

Fig. 1. (a) FTIR spectra, (b) DSC heat flow curves, (c) TG and (d) DTG curves of pure polymers and fiber reinforced composite laminates.

Table 2
Thermal properties of composites based on DSC and TGA.

Samples	T_g (°C)	wt% loss @ 150 °C	$T_{5\%}$ (°C)	T_{max} (°C)	Residual wt% @ 700°°C
Pure polymer	36.19	4.05	160.44	321.55	0.01
nFRP	38.28	3.75	186.53	335.36	7.08
nFRP-G1	35.89	2.49	228.24	336.21	14.95
nFRP-G2	35.50	1.86	231.14	337.52	16.76
nFRP-G3	35.21	2.81	208.77	338.04	17.91
gFRP	34.87	2.70	219.43	339.59	28.54

the dehydration of solvent materials and absorbed moisture (Hou et al., 2023). (2) The second major degradation appears between 250 °C and 400 °C, which is equivalent to a 70% decrease in weight. It was due to the depolymerization, dehydration, and decomposition of polymers, which result in char residue formation (Mahmud et al., 2020). The degradation of an organic-based sizing additive on the fiber may also be responsible for the mass loss at these temperatures (Aisyah et al., 2019). For coir fiber-reinforced samples, this degradation was also due to the decomposition of cellulose, hemicellulose, and lignin of natural fibers (Kumar et al., 2014). (3) The weight loss in the third phase in a linear pattern starts at 400 °C and corresponds to the left-over char residue's oxidation and successive decomposition into small volatile particles (Mahmud et al., 2019). Herein, the TGA curve of nFRP has not reached a stable state at 800 °C due to residual carbon in the material. Natural coir fibers contain a significant amount of lignin and cellulose, which are decomposed into carbon-rich residues during thermal degradation. The presence of these carbon residues can prevent the TGA curve from reaching a stable state even at high temperatures (Monteiro et al., 2012). Furthermore, the char yield of the composite samples at the end of the TGA experiment was increased compared with the pure polymer. Flame resistance is positively correlated with the increase in char yield (Kuang et al., 2023). As a result, increased char creation can lower the exothermicity of the pyrolysis reaction, hinder the production of combustible gas, and inhibit the thermal conductivity of burning items (Shi et al., 2012).

3.2. Mechanical properties

Mechanical properties of FRP composite laminates can be controlled by numerous factors such as the ply stacking sequency, fiber orientation, fiber volume fraction, and porosity. Herein, mechanical properties were observed based on the types of fibers and their stacking sequence in the panel through a three-point bending test. Typical load-deflection curves of composites are shown in Fig. 2, and the data are summarized in Table 3. The composites made of neat glass fabric (gFRP) and pure natural coir fibers (nFRP) possess the highest (~112.5 MPa) and lowest (~5.5 MPa) flexural strength values, corresponding to their individual fiber strength, respectively. It was due to the higher tensile strength of glass fibers than coir fibers. The hybridized fiber reinforced composites (nFRP-G1, nFRP-G2, and nFRP-G3) have a flexural strength of around ~ 26 MPa, which was about five folds higher than nFRP due to the leverage of the load carrying capability of glass fabrics. In the hybrid composite, the strongest glass fabrics at the outer layers carry the maximum possible stress during the three-point bending test. Hence, the

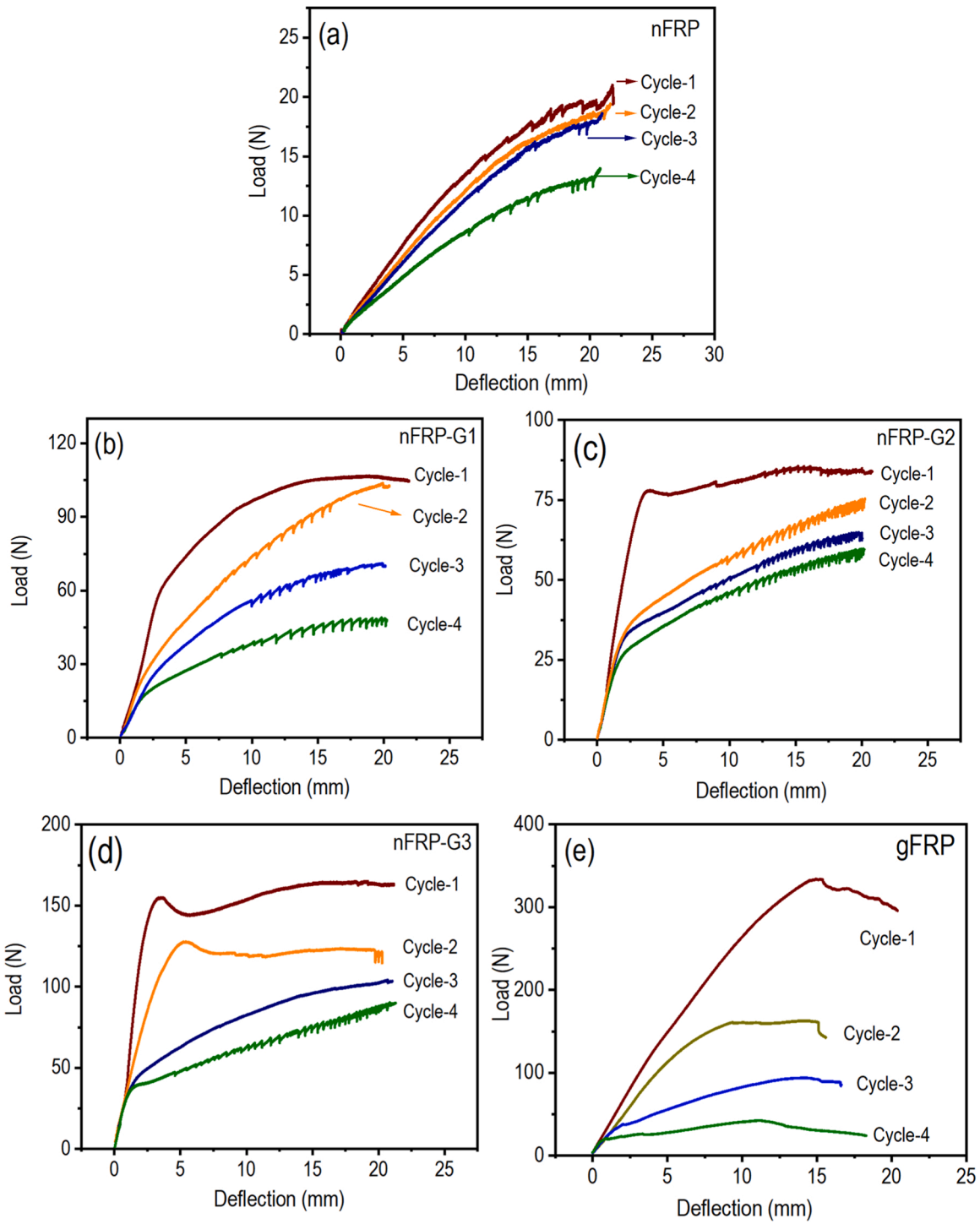

Fig. 2. Typical load *vs.* deflection curve of three-point bending test: (a) nFRP, (b) nFRP-G1, (c) nFRP-G2, (d) nFRP-G3, and (e) gFRP laminate composites (The test cycles 1, 2, 3 and 4 were conducted after 0, 1, 2 and 3 cycles of damage/healing, respectively).

Table 3
Mechanical properties of composites based on three-point bending and low-velocity impact test.

Samples	Flexural Strength (MPa)	Max Impact Force (kN)	Initiation Energy (J)	Max Impact Energy (J)	Propagation Energy (J)	Ductility Index (DI)
nFRP	5.53 ± 0.11	0.189 ± 0.000	0.175 ± 0.035	2.556 ± 0.135	2.382 ± 0.100	13.61
nFRP-G1	25.90 ± 3.23	0.845 ± 0.015	2.488 ± 0.356	10.828 ± 0.024	8.341 ± 0.379	3.35
nFRP-G2	22.60 ± 2.05	0.877 ± 0.001	2.995 ± 0.027	11.667 ± 0.147	8.672 ± 0.120	2.90
nFRP-G3	26.35 ± 3.59	0.909 ± 0.233	1.737 ± 0.720	11.168 ± 1.014	9.431 ± 0.294	5.43
gFRP	112.32 ± 30.63	1.485 ± 0.023	6.105 ± 0.190	13.631 ± 0.249	7.526 ± 0.059	1.23

glass fibers are utilized to resist compressive and tensile stress (Prabhu et al., 2022; TG et al., 2022; Wang et al., 2020a). The neat coir fiber reinforced (nFRP) composite has lower flexural strength and load values due to the inability in stress transfer of the short fibers that are loosely interlocked in random direction in the mat, resulting in the lowest load-bearing ability of the composites (TG et al., 2022). In summary, such a stacking sequence of fibers in the composites nicely adopted the flexural stress distribution, i.e., the normal stress is the highest on the top and bottom layers but is zero at the mid-plane, with a (non)linear slope, correspondingly, the top and bottom-most layers with strongest glass fibers and the layers adjacent to the midplane with the weakest natural coir fibers. Although the shear stress is the highest at the mid-plane under a three-point bending load, it may not be a major concern as most materials can survive the higher shear stress.

In addition to the static three-point bending test, the low-velocity impact test has also been conducted. Fig. 3 depicts the load *vs*. time plot to explain how dynamic load is applied to the composites by the impactor during a typical low-velocity impact test. The load *vs*. time curve of gFRP composites in the first cycle impact consists of an ascending portion of loading until the peak force is reached, followed by a descending portion of unloading. The slight oscillations in the curve indicate the probability of material damage due to decreased stiffness; however, the absence of any sharp force drop indicates that the composite was more resistant to low-velocity impact. Obviously, the peak force on the curve was a crucial metric for determining the impact load capacity of the composite laminates. Before reaching the peak force value, the overall trend on the curve depicts the elastic response of the composite laminates. After achieving the maximal force value, the absence of a sudden drop in force indicates the absence of perforation in the composite laminates. This is a typical impact response of glass fiber-reinforced composite (Sun et al., 2018). On the other hand, the typical load *vs*. time plots for the coir fiber laminates (nFRP) impacted up to penetration demonstrate a sudden load drop due to the incident of damage with the onset of delamination, which indicates a sudden loss in

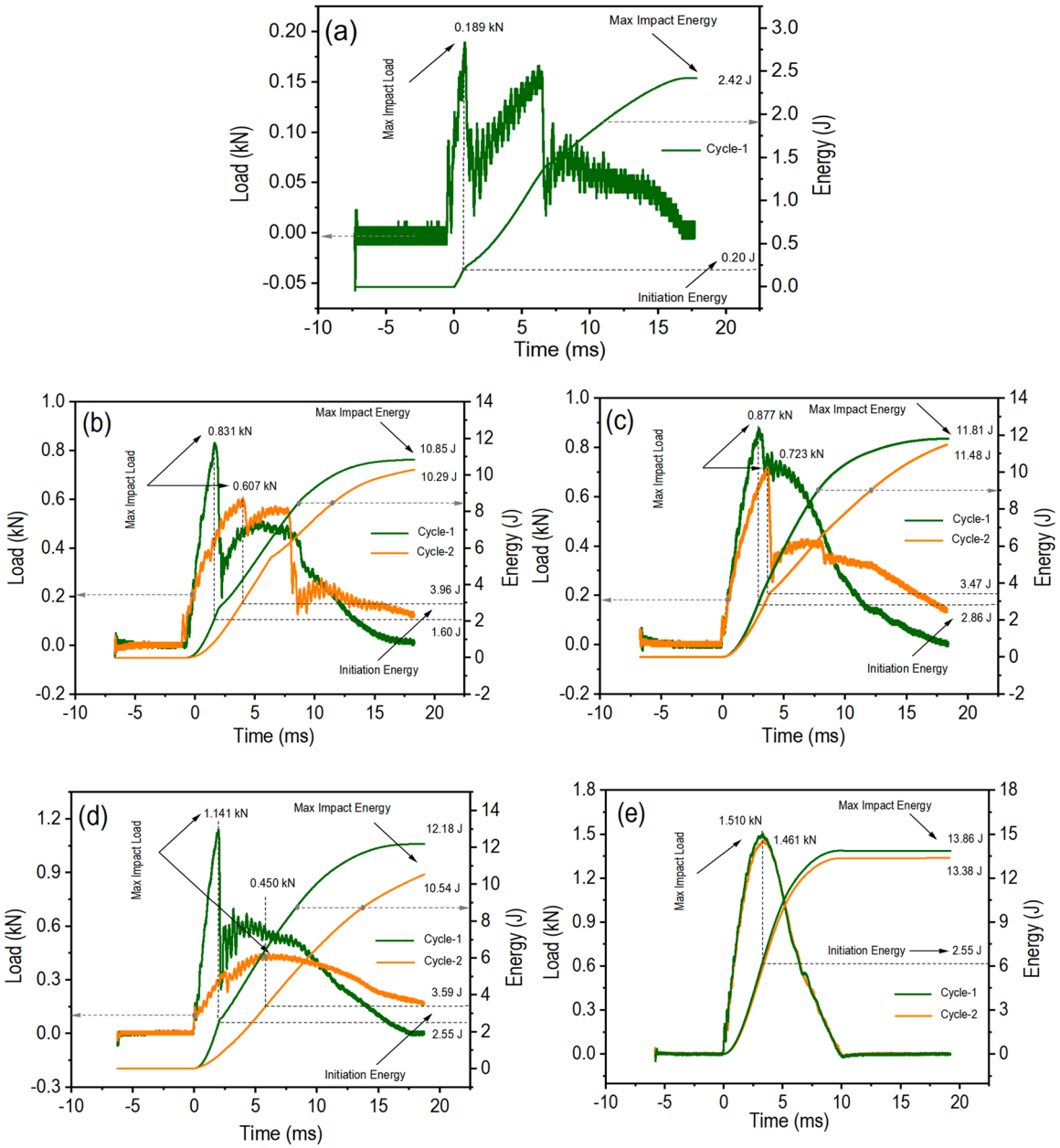

Fig. 3. Typical load and energy traces of low-velocity impact test: (a) nFRP, (b) nFRP-G1, (c) nFRP-G2, (d) nFRP-G3, and (e) gFRP laminate composites. (The test cycles 1 and 2 were conducted after 0 and 1 cycles of damage healing, respectively).

stiffness, after reaching the maximum load point. This peak load reflects the maximum load that the laminate can withstand before experiencing substantial damage. After this initial failure, the curve oscillated upwards until it reached its second maximum value and suddenly dropped again; an irregular plateau with many oscillations occurred, usually attributed to significant internal damage propagation. These results indicate the poor damage resistance of natural fiber composites when subjected to low-velocity impacts, which has been previously demonstrated by other researchers (Ahmed et al., 2007; Scarponi et al., 2016). Although a similar pattern of load change was observed in glass/coir hybrid fibers composites (nFRP-G1, nFRP-G2, and nFRP-G3), they demonstrate significantly different maximum impact load. All glass fiber laminates exhibit the highest stiffness, whereas coir fibers reinforced composites demonstrate the lowest possible stiffness. All hybrid composite laminates present stiffness that is evidently higher than the coir fibers but closer to the glass fiber laminates. From all the graphs, it could notice a proportional correlation between the peak impact load and the number of glass fabric layers in the laminates.

It is recognized that the peak impact force, initiation energy, and propagation energy during impact are the major factors to assess the impact tolerance. Notably, propagation energy is the quantity of energy experienced by the object during the propagation of massive damage. In contrast, the initiation energy is essentially a measurement of a target's ability to transfer energy elastically (Konlan et al., 2020). The impact energy associate to the peak impact force is known as the initiation energy. The propagation energy is determined by subtracting the initiation energy from the maximal impact energy (Li and John, 2008). Higher initiation energy and lower propagation energy indicate that the composite laminate can withstand impact to a greater extent. In simple words, the impact tolerance increases with increasing initiation energy and decreasing propagation energy. Higher propagation energy observed during the test typically predicts enormous impact damage. Therefore, initiation and propagation energy are summarized in Table 3 based on typical energy-time responses (Fig. 3) under the low-velocity impact of the glass and coir fibers composite laminates and their hybrids.

Accordingly, the following conclusions can be drawn. (a) the glass fiber composite laminates show significantly higher impact tolerance than coir fibers as indicated by the much higher maximum impact force and initiation energy. In addition, the higher propagation energy of gFRP composite laminates suggests the absorption of more energy through damage. (b) The addition of glass fiber layers on the nFRP composite laminates proportionally increased the maximum impact force and initiation energy, indicating a parallel enhancement in impact tolerance. Again, the rise in propagation energy due to the incorporation of glass fiber layers on nFRP suggests the damage in these hybrid composites is likely due to delamination. As will be discussed in the next section, this is indeed the case. Delamination and matrix cracking are the dominating failure modes. No fiber fracture is observed in the hybrid composites. Delamination is healable, but fiber fracture is not. Moreover, as evidenced by the impact load and energy versus time curves, the failure process could begin at the maximum load point for a hybrid composite. Therefore, it may be more meaningful to use the ductility index (DI) to understand the ductility of the composite. The DI can be calculated as the ratio of propagation energy and the initiation energy, and a higher value indicates a more ductile composite (Wang et al., 2008). The DI values of the investigated laminates as listed in Table 3 indicates that the addition of natural coir fibers in the gFRP markedly increases the ductility. In particular, the DI values of the hybrid composites was about 2–4 times that of the gFRP. A similar finding was also observed by Salehi-Khojin et al. (Salehi-Khojin et al., 2006). Of course, the nFRP has the highest DI value, suggesting the most ductile composite, which is also aligned with its bending test.

Although the nFRP has the highest DI, its energy absorption is not through delamination or matrix cracking; instead, it is through fiber fracture. The impact force on the nFRP composite laminates caused the fracture of the sample into several pieces (so these samples were not possible to move on for healing) (Fig. 4**a**). It was due to the weak mechanical strength of the coir fibers, small fiber aspect ratio, and random distribution of the coir fiber in the mat. It results in insufficient stress transfer through the matrix to the reinforcement that reflects the lower maximum impact load compared with the other samples (Table 3). The damage mechanism of fiber-reinforced composite laminates is extremely complex. In the case of composites, impact-induced damage frequently begins on the back surface or as internal damage (Bieniaś et al., 2015). In the case of the nFRP, the damage is not due to matrix dominated damage such as delamination and matrix cracking, but due to more critical damage, fiber fracture. Unfortunately, fractured fibers cannot be healed. This is the reason only one impact cycle was conducted on the nFRP. In the case of hybrid composite laminates, the impact force induces some acute angle transverse cracks and delamination in the impact area (Fig. 4**b-d**). Although both the hybrid (Fig. 4**b-d**) and gFRP (Fig. 4**e**) composite laminates apparently reveal similar fracture patterns, i.e., transvers shear crack and delamination, the crack opening is clearly larger in the hybrid composite than that in the pure glass composite, which is echoed by the slightly lower peak impact force and lower initiation energy in the hybrid composites. Although the hybrid composites have slightly lower impact tolerance than the pure glass fiber reinforced composite, the damages can be healed because both transverse shear cracking and delamination are induced by matrix failure.

3.3. Room temperature healing properties

It is clear from the previous section that the composite laminates are vulnerable under the impact. The extreme interlaminar shear stress causes matrix cracking and delamination. Hence, the low-velocity impact test on composite laminates has been performed again to understand the self-healing properties at room temperature. The composite laminates were first impacted to produce crack and delamination and subsequently healed at room temperature under 5 MPa pressure for 12 h. The healed composite samples were resubjected to the low-velocity impact test at the same location and test condition. Initially, the microscopic image before and after healing was captured, and analysis of the bending-induced matrix cracks and visible delamination was conducted (Fig. 5). It was observed that the wide-opened delamination and the cracks in the matrix had been reduced and almost disappeared after compression at room temperature, indicating the fractured samples were nicely healed. To numerically analyze the healing efficiency, the impact forces before and after the healing of composite laminates were tested under the same test condition (Fig. 4 and Table S2). The impact load of the virgin specimens of nFRP-G1, nFRP-G2, nFRP-G3, and gFRP reached ~0.845 kN in 1.61 ms, ~0.877 kN in 2.97 ms, ~0.909 kN in 1.97 ms, and ~1.485 kN in 3.15 ms, while after healing the sample reached to ~0.573 kN in 3.99 ms, ~0.751 kN in 3.83 ms ~0.544 kN in 5.77 ms, and ~1.478 kN in 3.43 ms, respectively. It means the impact load of the healed samples gets close to the impact load of the virgin samples but requires a bit longer time. It literally signifies that the stiffness and strength of the laminates were also restored after the healing process. The healing efficiency after the first impact of nFRP-G1, nFRP-G2, nFRP-G3, and gFRP were calculated to be 67.77%, 85.66%, 59.87%, and 99.56%, respectively (Fig. 6b). It is worth mentioning that the coir fibers in the hybrid composite laminates fractured after the second impact; therefore, the repetition of impact and healing was stopped after second impact. However, the gFRP survived up to the fifth impact cycle with 83.30% of healing efficiency (Fig. S2), implying an excellent self-healing ability of the composites. In addition to employing maximum impact force as a criterion for determining the healing efficiency, other parameters like propagation energy produced by impact force may also be employed (Fig. 2 and Table S1). Because the nFRP composites were completely fractured after one impact and was not healable, we also used bending test to assess the healing efficiency. Similarly, the flexural strengths

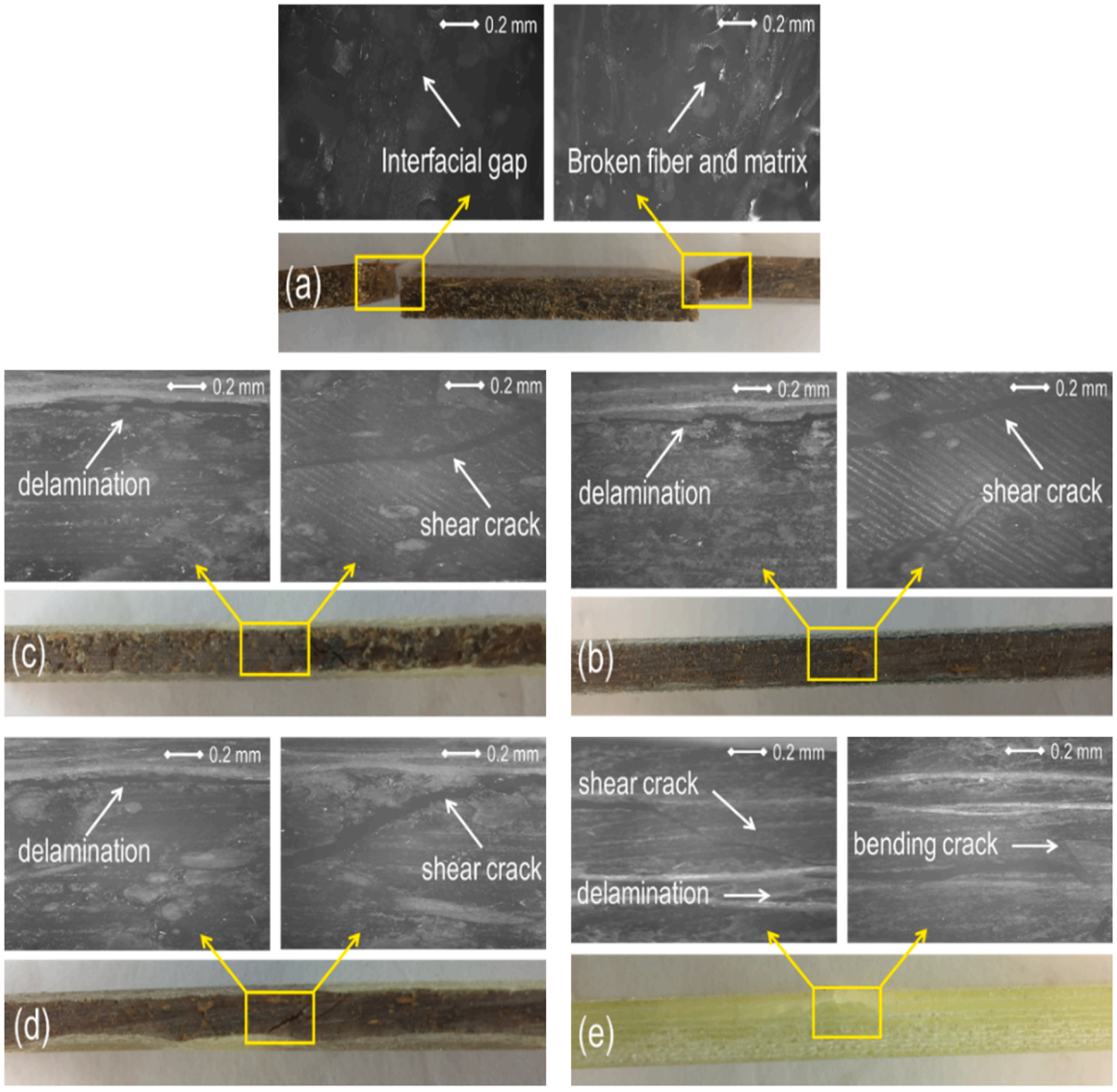

Fig. 4. Typical failure of laminates after low-velocity impact: (a) nFRP, (b) nFRP-G1, (c) nFRP-G2, (d) nFRP-G3, and (e) gFRP laminate composites.

were used as a parameter to assess the healing efficiency up to four cycles (Fig. 6a and Table S1). The results show a systematic drop of the flexure strength and the healing efficiency as the bending and healing cycle increased, i.e., a common tendency of fiber reinforced laminate composites (Heo and Sodano, 2015).

The healing properties were associated with the polymer used, where a branched PEI, and an ester-rich DCN epoxy monomer was covalently and mildly crosslinked in a nonstoichiometric proportion. As discussed in previous report (Feng and Li, 2021b), the polymer has two healing mechanisms: through hydrogen bonds at room temperature (below the T_g) and through transesterification reaction at temperature above the T_g. This research further proves the healing capability of the polymer in glassy state, even with natural fibers. The reason for the dropping of the healing efficiency with damage/healing cycles, which is common for self-healing composites, is obvious. With the increase in the damage healing cycles, some unhealable damage will accumulate, such as fiber fracture, fracture of non-reversible covalent bonds, etc. As a result, the healing efficiency decreases gradually with the increase in the damage/healing cycles.

3.4. Shape memory effect

In this study, the DCN-PEI thermoset polymer has shape memory effect. As a result, the composite laminates should also have shape memory capabilities. To evaluate the shape memory effect, their crucial factors, such as the shape fixity ratio and shape recovery ratio, were calculated (Table S2 and Fig. 7a-b). The average values of shape fixity ratios for nFRP, nFRP-G1, nFRP-G2, nFRP-G3, and gFRP composite laminates were 16.90%, 51.05%, 32.56%, 36.50%, and 30.14%, respectively. In addition, their shape recovery ratios were 82.57%, 91.73%, 86.95%, 87.99%, and 93.49%, respectively. First, all the composites have very high recovery ratios, suggesting good shape memory effect. However, the shape fixity ratio is low, mainly due to the incorporation of the elastic fibers. During room temperature programming, unloading is companied by a large spring-back due to the elasticity of the reinforcing fibers. Therefore, all the composites show a low shape fixity ratio. Among all composite laminates, the nFRP showed comparatively lower performance, possibly due to the random orientation of the natural fibers in the composites (Korotkov et al., 2021). It was also observed that even after five shape memory cycles, all composite laminates gradually decreased but maintained a good shape recovery ratio and shape fixity ratio compared with the first rounds. Overall, the

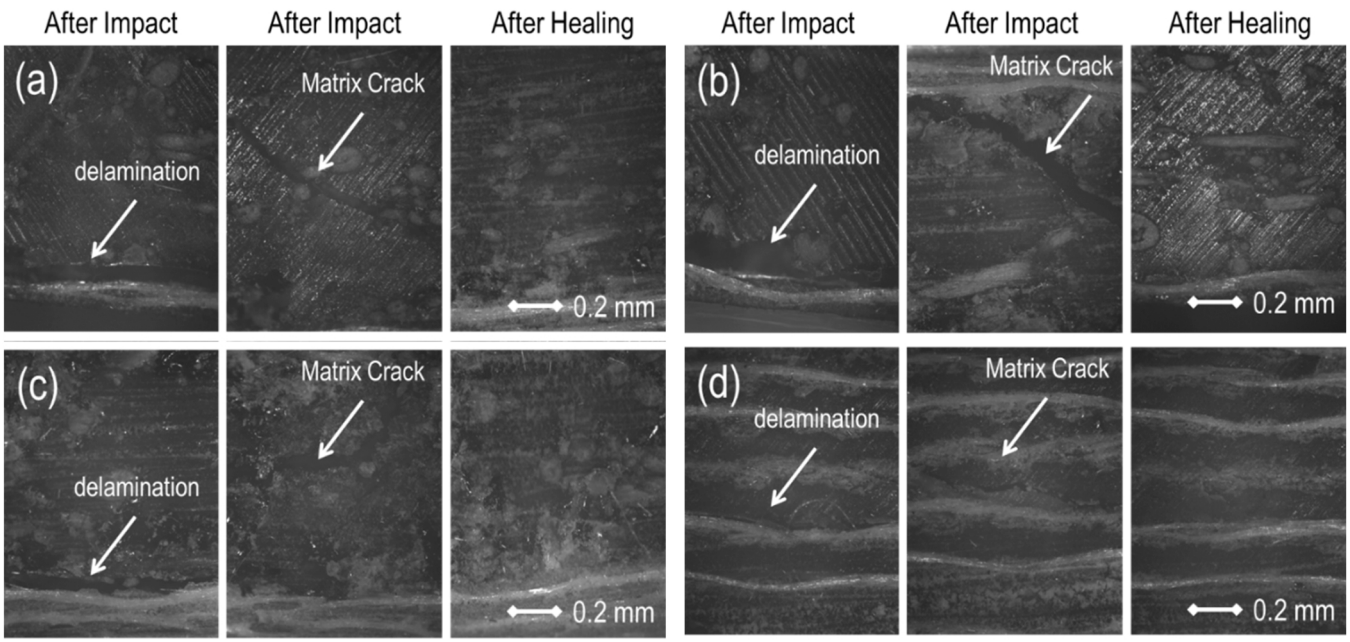

Fig. 5. Microscopic images of composite laminates after impact (left and middle column) and after healing (right column): (a) nFRP-G1, (b) nFRP-G2, (c) nFRP-G3, and (d) gFRP laminate composites.

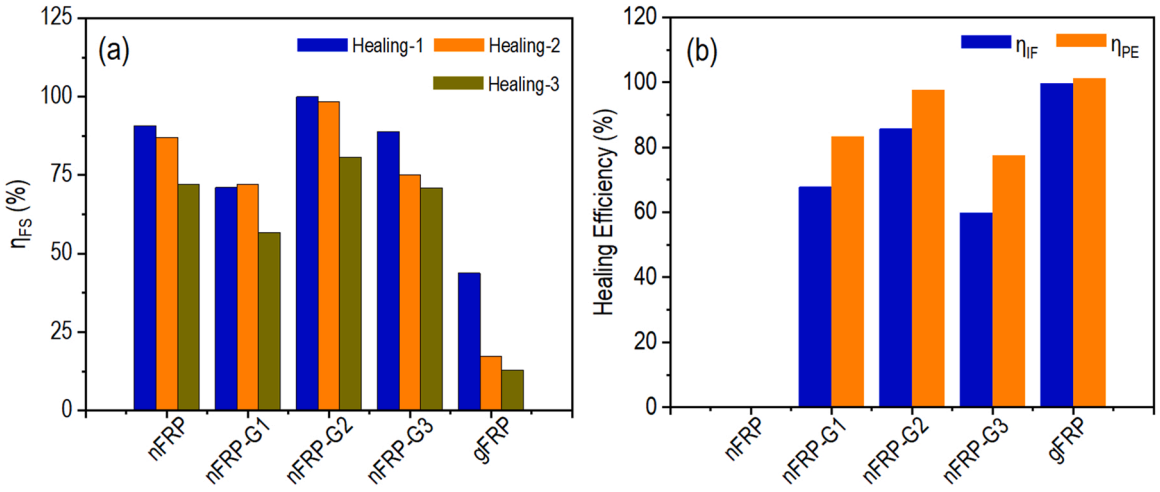

Fig. 6. (a) Healing efficiency (η_{FS}) based on three-point bending tests, and (b) healing efficiency based on impact force (η_{IF}), and propagation energy (η_{PE}).

shape memory polymer system used in this work was suitable for serving as a matrix for hybrid fiber reinforced composite laminates.

4. Conclusions

Fiber-reinforced polymer composite laminates were fabricated using newly synthesized self-healing shape memory DCN-PEI polymers by stacking synthetic glass fibers over the core of natural coir fiber. Due to the (non)linear distribution of normal strain, even with a significant portion of coir fibers in the composites in the core, the hybrid composites show about five times increase in bending strength as compared with the pure coir fiber reinforced composite. Under the static bending test, the hybrid composites' damage is healed repeatedly at room temperature, with healing efficiencies of 99% during the first healing cycle and 72% for the fourth. Also, the hybrid composites have good shape memory behavior, with shape fixity of up to 51% and shape recovery ratio of up to 93%. Even under low-velocity impact tests, the hybrid composites can be healed more than one time, while the pure coir fiber composite fractured into pieces under the first impact cycle. Because of the dual mechanisms in the self-healing of the polymer matrix, it is shown that matrix-dominated damage (such as transverse shear crack and in-plane delamination) can be healed repeatedly at room temperature, regardless of the load causing damage (static load or impact load). This study shows that natural fibers, when used in hybrid form with a small volume fraction of synthetic fibers, can lead to composites with comparable functional properties to those reinforced by pure synthetic fiber alone. Combined with a smart polymer matrix, natural fibers can be used in composite materials with potential applications in lightweight structures.

CRediT authorship contribution statement

SM conducted composite preparation and testing and wrote the first draft of the manuscript; JK participated in composite preparation and testing; JD participated in composite preparation and testing; GL conceptualized and supervised the research, obtained funding, and

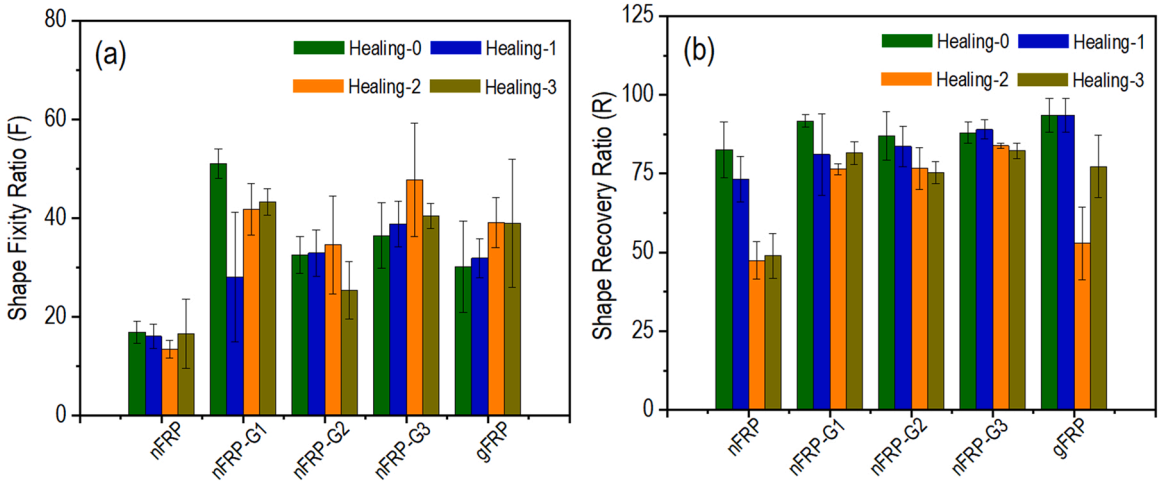

Fig. 7. (a) Shape fixity ratio, and (b) shape recovery ratio based on three-point bending tests.

revised the manuscript.

Declaration of Competing Interest

The authors declare that they have no known competing financial interests or personal relationships that could have appeared to influence the work reported in this paper.

Data Availability

Data will be made available on request.

Acknowledgment

This work is supported by the US National Science Foundation under Grant Number OIA-1946231 and the Louisiana Board of Regents for the Louisiana Materials Design Alliance (LAMDA), and National Science Foundation under grant number 1736136.

Appendix A. Supporting information

Supplementary data associated with this article can be found in the online version at doi:10.1016/j.indcrop.2023.116895.

References

Abrão, A.M., Faria, P.E., Rubio, J.C., Reis, P., Davim, J.P., 2007. Drilling of fiber reinforced plastics: a review. J. Mater. Process. Technol. 186, 1–7. https://doi.org/10.1016/j.jmatprotec.2006.11.146.

Ahmed, K.S., Vijayarangan, S., Kumar, A., 2007. Low velocity impact damage characterization of woven jute—glass fabric reinforced isothalic polyester hybrid composites. J. Reinf. Plast. Compos 26, 959–976. https://doi.org/10.1177/0731684407079414.

Aisyah, H., Paridah, M., Sapuan, S., Khalina, A., Berkalp, O., Lee, S., Lee, C., Nurazzi, N., Ramli, N., Wahab, M., 2019. Thermal properties of woven kenaf/carbon fibre-reinforced epoxy hybrid composite panels. Int. J. Polym. Sci. https://doi.org/10.1155/2019/5258621.

Arockiasamy, F.S., M, M., 2022. Experimental investigation on the effect of fiber volume fraction of sponge gourd outer skin fiber reinforced epoxy composites. Polym. Compos. 43, 6932–6942. https://doi.org/10.1002/pc.26754.

Basak, S., 2021. Redesigning the modern applied medical sciences and engineering with shape memory polymers. Adv. Compos Hybrid. Mater. 4, 223–234. https://doi.org/10.1007/s42114-021-00216-1.

Bieniaś, J., Jakubczak, P., Surowska, B., Dragan, K., 2015. Low-energy impact behaviour and damage characterization of carbon fibre reinforced polymer and aluminium hybrid laminates. Arch. Civ. Mech. Eng. 15, 925–932. https://doi.org/10.1016/j.acme.2014.09.007.

Bonon, A.J., Weck, M., Bonfante, E.A., Coelho, P.G., 2016. Physicochemical characterization of three fiber-reinforced epoxide-based composites for dental applications. Mater. Sci. Eng. C. 69, 905–913. https://doi.org/10.1016/j.msec.2016.07.002.

Chen, F., Xiao, H., Peng, Z.Q., Zhang, Z.P., Rong, M.Z., Zhang, M.Q., 2021. Thermally conductive glass fiber reinforced epoxy composites with intrinsic self-healing capability. Adv. Compos Hybrid. Mater. 4, 1048–1058. https://doi.org/10.1007/s42114-021-00303-3.

Cho, D., Lee, H.S., Han, S.O., 2009. Effect of fiber surface modification on the interfacial and mechanical properties of kenaf fiber-reinforced thermoplastic and thermosetting polymer composites. Compos. Interfaces 16, 711–729. https://doi.org/10.1163/092764409×12477427307537.

Feng, X., Li, G., 2021a. Catalyst-free β-hydroxy phosphate ester exchange for robust fire-proof vitrimers. Chem. Eng. J. 417, 129132 https://doi.org/10.1016/j.cej.2021.129132.

Feng, X., Li, G., 2021b. Room-temperature self-healable and mechanically robust thermoset polymers for healing delamination and recycling carbon fibers. ACS Appl. Mater. Interfaces 13, 53099–53110. https://doi.org/10.1021/acsami.1c16105.

Feng, X., Fan, J., Li, A., Li, G., 2019. Multireusable thermoset with anomalous flame-triggered shape memory effect. ACS Appl. Mater. Interfaces 11, 16075–16086. https://doi.org/10.1021/acsami.9b03092.

Feni, F., Jahan, M., Dawan, F., Ibekwe, S., Li, G., Mensah, P., 2022. Enhancing the mechanical performance of carbon fiber reinforced polymer using carbonized coconut shell particles. Mater. Today Commun. 33, 104727 https://doi.org/10.1016/j.mtcomm.2022.104727.

Forintos, N., Czigany, T., 2019. Multifunctional application of carbon fiber reinforced polymer composites: electrical properties of the reinforcing carbon fibers–A short review. Compos. B. Eng. 162, 331–343. https://doi.org/10.1016/j.compositesb.2018.10.098.

Fouladi, M.H., Ayub, M., Nor, M.J.M., 2011. Analysis of coir fiber acoustical characteristics. Appl. Acoust. 72, 35–42. https://doi.org/10.1016/j.apacoust.2010.09.007.

Grund, D., Orlishausen, M., Taha, I., 2019. Determination of fiber volume fraction of carbon fiber-reinforced polymer using thermogravimetric methods. Polym. Test. 75, 358–366. https://doi.org/10.1016/j.polymertesting.2019.02.031.

Haafiz, M.M., Hassan, A., Zakaria, Z., Inuwa, I.M., Islam, M.S., Jawaid, M., 2013. Properties of polylactic acid composites reinforced with oil palm biomass microcrystalline cellulose. Carbohydr. Polym. 98, 139–145.

Haris, N.I.N., Ilyas, R., Hassan, M.Z., Sapuan, S., Afdzaluddin, A., Jamaludin, K.R., Zaki, S.A., Ramlie, F., 2021. Dynamic mechanical properties and thermal properties of longitudinal basalt/woven glass fiber reinforced unsaturated polyester hybrid composites. Polymers 13, 3343. https://doi.org/10.3390/polym13193343.

Heo, Y., Sodano, H.A., 2015. Thermally responsive self-healing composites with continuous carbon fiber reinforcement. Compos. Sci. Technol. 118, 244–250. https://doi.org/10.1016/j.compscitech.2015.08.015.

Hou, C., Yang, W., Kimura, H., Xie, X., Zhang, X., Sun, X., Yu, Z., Yang, X., Zhang, Y., Wang, B., Xu, B.B., Sridhar, D., Algadi, H., Guo, Z., Du, W., 2023. Boosted lithium storage performance by local build-in electric field derived by oxygen vacancies in 3D holey N-doped carbon structure decorated with molybdenum dioxide. J. Mater. Sci. Technol. 142, 185–195. https://doi.org/10.1016/j.jmst.2022.10.007.

Kerni, L., Singh, S., Patnaik, A., Kumar, N., 2020. A review on natural fiber reinforced composites. Mater. Today Proc. 28, 1616–1621. https://doi.org/10.1016/j.matpr.2020.04.851.

Khan, Z.I., Arsad, A., Mohamad, Z., Habib, U., Zaini, M.A.A., 2021. Comparative study on the enhancement of thermo-mechanical properties of carbon fiber and glass fiber reinforced epoxy composites. Mater. Today Proc. 39, 956–958. https://doi.org/10.1016/j.matpr.2020.04.223.

Konlan, J., Mensah, P., Ibekwe, S., Crosby, K., Li, G., 2020. Vitrimer based composite laminates with shape memory alloy Z-pins for repeated healing of impact induced delamination. Compos. B. Eng. 200, 108324 https://doi.org/10.1016/j.compositesb.2020.108324.

Konlan, J., Mensah, P., Ibekwe, S., Li, G., 2022. A laminated vitrimer composite with strain sensing, delamination self-healing, deicing, and room-temperature shape

restoration properties. J. Compos. Mater. 56, 2267–2278. https://doi.org/10.1177/00219983221098225.
Korotkov, R., Vedernikov, A., Gusev, S., Alajarmeh, O., Akhatov, I., Safonov, A., 2021. Shape memory behavior of unidirectional pultruded laminate. Compos. Part A Appl. Sci. 150, 106609 https://doi.org/10.1016/j.compositesa.2021.106609.
Kuang, T., Zhang, M., Chen, F., Fei, Y., Yang, J., Zhong, M., Wu, B., Liu, T., 2023. Creating poly(lactic acid)/carbon nanotubes/carbon black nanocomposites with high electrical conductivity and good mechanical properties by constructing a segregated double network with a low content of hybrid nanofiller. Adv. Compos Hybrid. Mater. 6, 48. https://doi.org/10.1007/s42114-022-00622-z.
Kumar, S.S., Duraibabu, Da, Subramanian, K., 2014. Studies on mechanical, thermal and dynamic mechanical properties of untreated (raw) and treated coconut sheath fiber reinforced epoxy composites. Mater. Des. 59, 63–69. https://doi.org/10.1016/j.matdes.2014.02.013.
Li, A., Fan, J., Li, G., 2018. Recyclable thermoset shape memory polymers with high stress and energy output via facile UV-curing. J. Mater. Chem. A 6, 11479–11487. https://doi.org/10.1039/C8TA02644K.
Li, G., John, M., 2008. A self-healing smart syntactic foam under multiple impacts. Compos. Sci. Technol. 68, 3337–3343. https://doi.org/10.1016/j.compscitech.2008.09.009.
Li, P., Wang, X., Su, M., Zou, X., Duan, L., Zhang, H., 2021. Characteristics of plastic pollution in the environment: a review. Bull. Environ. Contam. Toxicol. 107, 577–584. https://doi.org/10.1007/s00128-020-02820-1.
Lu, L., Pan, J., Li, G., 2017. Recyclable high-performance epoxy based on transesterification reaction. J. Mater. Chem. A 5, 21505–21513. https://doi.org/10.1039/C7TA06397K.
MacLeod, M., Arp, H.P.H., Tekman, M.B., Jahnke, A., 2021. The global threat from plastic pollution. Science 373, 61–65.
Mahmud, S., Long, Y., Yang, Y., Huang, J., Zhang, R., Zhu, J., 2019. The consequence of epoxidized soybean oil in the toughening of polylactide and micro-fibrillated cellulose blend. Polym. Sci. Ser. A 61, 832–846. https://doi.org/10.1134/S0965545×2001006X.
Mahmud, S., Wang, J., Shao, N., Xiong, Z., Zhang, R., Zhu, J., 2020. Nucleation and crystallization of poly (propylene 2, 5-furan dicarboxylate) by direct blending of microcrystalline cellulose: improved tensile and barrier properties. Cellulose 27, 9423–9436. https://doi.org/10.1007/s10570-020-03448-4.
Mazumdar, S., Karthikeyan, D., Pichler, D., Benevento, M., Frassine, R., 2017. State of the composites industry report for 2017. Compos. Manuf. Mag. 2.
Monteiro, S.N., Lopes, F.P.D., Ferreira, A.S., Nascimento, D.C.O., 2009. Natural-fiber polymer-matrix composites: cheaper, tougher, and environmentally friendly. Jom 61, 17–22. https://doi.org/10.1007/s11837-009-0004-z.
Monteiro, S.N., Calado, V., Rodriguez, R.J.S., Margem, F.M., 2012. Thermogravimetric behavior of natural fibers reinforced polymer composites—an overview. Mater. Sci. Eng. A 557, 17–28. https://doi.org/10.1016/j.msea.2012.05.109.
Mortazavian, S., Fatemi, A., 2015. Effects of fiber orientation and anisotropy on tensile strength and elastic modulus of short fiber reinforced polymer composites. Compos. B. Eng. 72, 116–129. https://doi.org/10.1016/j.compositesb.2014.11.041.
Nji, J., Li, G., 2010. A biomimic shape memory polymer based self-healing particulate composite. Polymer 51, 6021–6029. https://doi.org/10.1016/j.polymer.2010.10.021.
Nji, J., Li, G., 2012. Damage healing ability of a shape-memory-polymer-based particulate composite with small thermoplastic contents. Smart Mater. Struct. 21, 025011 https://doi.org/10.1088/0964-1726/21/2/025011.
Ouyang, L., Huang, W., Huang, M., Qiu, B., 2022. Polyaniline improves granulation and stability of aerobic granular sludge. Adv. Compos Hybrid. Mater. 5, 1126–1136. https://doi.org/10.1007/s42114-022-00450-1.
Post, W., Susa, A., Blaauw, R., Molenveld, K., Knoop, R.J., 2020. A review on the potential and limitations of recyclable thermosets for structural applications. Polym. Rev. 60, 359–388. https://doi.org/10.1080/15583724.2019.1673406.
Prabhu, L., Krishnaraj, V., Gokulkumar, S., Sathish, S., Sanjay, M., Siengchin, S., 2022. Mechanical, chemical and sound absorption properties of glass/kenaf/waste tea leaf fiber-reinforced hybrid epoxy composites. J. Ind. Text. 51, 1674–1700. https://doi.org/10.1177/1528083720957392.
Prasad, N., Agarwal, V.K., Sinha, S., 2018. Thermal degradation of coir fiber reinforced low-density polyethylene composites. Sci. Eng. Compos. Mater. 25, 363–372. https://doi.org/10.1515/secm-2015-0422.
Putnam-Neeb, A.A., Kaiser, J.M., Hubbard, A.M., Street, D.P., Dickerson, M.B., Nepal, D., Baldwin, L.A., 2022. Self-healing and polymer welding of soft and stiff epoxy thermosets via silanolates. Adv. Compos Hybrid. Mater. 5, 3068–3080. https://doi.org/10.1007/s42114-022-00558-4.
Rajadurai, A., 2017. Inter laminar shear strength behavior of acid, base and silane treated E-glass fibre epoxy resin composites on drilling process. Def. Technol. 13, 40–46. https://doi.org/10.1016/j.dt.2016.11.004.
Reddy, B.M., Mohana Reddy, Y.V., Mohan Reddy, B.C., Reddy, R.M., 2020. Mechanical, morphological, and thermogravimetric analysis of alkali-treated Cordia-Dichotoma natural fiber composites. J. Nat. Fibers 17, 759–768. https://doi.org/10.1080/15440478.2018.1534183.
Salehi-Khojin, A., Bashirzadeh, R., Mahinfalah, M., Nakhaei-Jazar, R., 2006. The role of temperature on impact properties of Kevlar/fiberglass composite laminates. Compos. B. Eng. 37, 593–602. https://doi.org/10.1016/j.compositesb.2006.03.009.
Sathishkumar, T., Satheeshkumar, S., Naveen, J., 2014. Glass fiber-reinforced polymer composites–a review. J. Reinf. Plast. Compos 33, 1258–1275. https://doi.org/10.1177/07316844145307.
Scarponi, C., Sarasini, F., Tirillò, J., Lampani, L., Valente, T., Gaudenzi, P., 2016. Low-velocity impact behaviour of hemp fibre reinforced bio-based epoxy laminates. Compos. B. Eng. 91, 162–168. https://doi.org/10.1016/j.compositesb.2016.01.048.
Scheutz, G.M., Lessard, J.J., Sims, M.B., Sumerlin, B.S., 2019. Adaptable crosslinks in polymeric materials: resolving the intersection of thermoplastics and thermosets. J. Am. Chem. Soc. 141, 16181–16196. https://doi.org/10.1021/jacs.9b07922.
Seghini, M., Touchard, F., Sarasini, F., Cech, V., Chocinski-Arnault, L., Mellier, D., Tirillò, J., Bracciale, M., Zvonek, M., 2019. Engineering the interfacial adhesion in basalt/epoxy composites by plasma polymerization. Compos. Part A Appl. Sci. 122, 67–76. https://doi.org/10.1016/j.compositesa.2019.04.013.
Sharafkhani, S., Kokabi, M., 2022. Enhanced sensing performance of polyvinylidene fluoride nanofibers containing preferred oriented carbon nanotubes. Adv. Compos Hybrid. Mater. 5, 3081–3093. https://doi.org/10.1007/s42114-022-00565-5.
Shi, Q., Zhou, C., Yue, Y., Guo, W., Wu, Y., Wu, Q., 2012. Mechanical properties and in vitro degradation of electrospun bio-nanocomposite mats from PLA and cellulose nanocrystals. Carbohydr. Polym. 90, 301–308. https://doi.org/10.1016/j.carbpol.2012.05.042.
Shiino, M.Y., Cipó, T.C.G., Donadon, M.V., Essiptchouk, A., 2021. Waste size and lay up sequence strategy for reusing/recycling carbon fiber fabric in laminate composite: mechanical property analysis. J. Compos. Mater. 55, 4221–4230. https://doi.org/10.1177/00219983211037047.
Sun, D., Yan, J., Ma, X., Lan, M., Wang, Z., Cui, S., Yang, J., 2021. Tribological investigation of self-healing composites containing metal/polymer microcapsules. ES Mater. Manuf. 14, 59–72. https://doi.org/10.30919/esmm5f469.
Sun, M., Chang, M., Wang, Z., Li, H., Sun, X., 2018. Experimental and simulation study of low-velocity impact on glass fiber composite laminates with reinforcing shape memory alloys at different layer positions. Appl. Sci. 8, 2405. https://doi.org/10.3390/app8122405.
TG, Y.G., Mavinkere Rangappa, S., Siengchin, S., Jawaid, M., 2022. Mechanical and thermal properties of flax/carbon/kevlar based epoxy hybrid composites. Polym. Compos. 43, 5649–5662. https://doi.org/10.1002/pc.26880.
Thangaraj, V., Mahmud, S., Li, W., Yang, F., Liu, H., 2017. Greenly synthesised silver-alginate nanocomposites for degrading dyes and bacteria. IET Nanobiotechnol. 12, 47–51. https://doi.org/10.1049/iet-nbt.2017.0074.
Van Zee, N.J., Nicolaÿ, R., 2020. Vitrimers: Permanently crosslinked polymers with dynamic network topology. Prog. Polym. Sci. 104, 101233 https://doi.org/10.1016/j.progpolymsci.2020.101233.
Verma, R., Vinoda, K., Papireddy, M., Gowda, A., 2016. Toxic pollutants from plastic waste-a review. Procedia Environ. Sci. 35, 701–708. https://doi.org/10.1016/j.proenv.2016.07.069.
Wang, A., Wang, X., Xian, G., 2020a. Mechanical, low-velocity impact, and hydrothermal aging properties of flax/carbon hybrid composite plates. Polym. Test. 90, 106759 https://doi.org/10.1016/j.polymertesting.2020.106759.
Wang, H., Liu, H., Cao, Z., Li, W., Huang, X., Zhu, Y., Ling, F., Xu, H., Wu, Q., Peng, Y., 2020b. Room-temperature autonomous self-healing glassy polymers with hyperbranched structure. Proc. Natl. Acad. Sci. 117, 11299–11305. https://doi.org/10.1073/pnas.2000001117.
Wang, X., Hu, B., Feng, Y., Liang, F., Mo, J., Xiong, J., Qiu, Y., 2008. Low velocity impact properties of 3D woven basalt/aramid hybrid composites. Compos. Sci. Technol. 68, 444–450. https://doi.org/10.1016/j.compscitech.2007.06.016.
Xu, J., Chen, J., Zhang, Y., Liu, T., Fu, J., 2021. A fast room-temperature self-healing glassy polyurethane. Angew. Chem. Int. Ed. 60, 7947–7955. https://doi.org/10.1002/anie.202017303.
Yanagisawa, Y., Nan, Y., Okuro, K., Aida, T., 2018. Mechanically robust, readily repairable polymers via tailored noncovalent cross-linking. Science 359, 72–76. https://doi.org/10.1126/science.aam7588.
Yang, R., He, Y., Zhang, H., 2016. Progress and trends in nondestructive testing and evaluation for wind turbine composite blade. Renew. Sustain. Energy Rev. 60, 1225–1250. https://doi.org/10.1016/j.rser.2016.02.026.
Zhang, Z., Zhao, Y., Li, Z., Zhang, L., Liu, Z., Long, Z., Li, Y., Liu, Y., Fan, R., Sun, K., Zhang, Z., 2022. Synthesis of carbon/SiO2 core-sheath nanofibers with Co-Fe nanoparticles embedded in via electrospinning for high-performance microwave absorption. Adv. Compos Hybrid. Mater. 5, 513–524. https://doi.org/10.1007/s42114-021-00350-w.
Zhu, Q., Zhao, Y., Miao, B., Abo-Dief, H.M., Qu, M., Pashameah, R.A., Xu, B.B., Huang, M., Algadi, H., Liu, X., Guo, Z., 2022. Hydrothermally synthesized ZnO-RGO-PPy for water-borne epoxy nanocomposite coating with anticorrosive reinforcement. Prog. Org. Coat. 172, 107153 https://doi.org/10.1016/j.porgcoat.2022.107153.